NASA TR R-58

NATIONAL AERONAUTICS AND SPACE ADMINISTRATION

NACA
TN 3934

TECHNICAL REPORT
R-58

CALCULATION OF AERODYNAMIC LOADING AND TWIST CHARACTERISTICS OF A FLEXIBLE WING AT MACH NUMBERS APPROACHING 1.0 AND COMPARISON WITH EXPERIMENT

By JOHN P. MUGLER, Jr.

1960

For sale by the Superintendent of Documents, U.S. Government Printing Office, Washington 25, D.C. Yearly subscription, $15: foreign, $19
single copy price varies according to size - - - - - - - - - Price 30 cents

TECHNICAL REPORT R-58

I. Mugler, John P., Jr. II. NASA TR R-58 NASA	NASA TR R-58. National Aeronautics and Space Administration. CALCULATION OF AERODYNAMIC LOADING AND TWIST CHARACTERISTICS OF A FLEXIBLE WING AT MACH NUMBERS APPROACHING 1.0 AND COMPARISON WITH EXPERIMENT. John P. Mugler, Jr. 1960. 1, 17 p. diagrs., tabs. GPO price 30 cents. (NASA TECHNICAL REPORT R-58.) An iteration method is presented by which the detailed aerodynamic loading and twist characteristics of a flexible wing with known elastic properties may be calculated. The method is applicable at Mach numbers approaching 1.0 as well as at subsonic Mach numbers. Calculations were made for a wing-body combination; the wing was swept back 45° and had an aspect ratio of 4. Comparisons were made with experimental results at Mach numbers from 0.80 to 0.98. (Initial NASA distribution: 1, Aerodynamics, aircraft; 3, Aircraft; 51, Stresses and loads). Copies obtainable from Sup't. of Docs., GPO, Washington	I. Mugler, John P., Jr. II. NASA TR R-58 NASA
I. Mugler, John P., Jr. II. NASA TR R-58 NASA	NASA TR R-58. National Aeronautics and Space Administration. CALCULATION OF AERODYNAMIC LOADING AND TWIST CHARACTERISTICS OF A FLEXIBLE WING AT MACH NUMBERS APPROACHING 1.0 AND COMPARISON WITH EXPERIMENT. John P. Mugler, Jr. 1960. 1, 17 p. diagrs., tabs. GPO price 30 cents. (NASA TECHNICAL REPORT R-58.) An iteration method is presented by which the detailed aerodynamic loading and twist characteristics of a flexible wing with known elastic properties may be calculated. The method is applicable at Mach numbers approaching 1.0 as well as at subsonic Mach numbers. Calculations were made for a wing-body combination; the wing was swept back 45° and had an aspect ratio of 4. Comparisons were made with experimental results at Mach numbers from 0.80 to 0.98. (Initial NASA distribution: 1, Aerodynamics, aircraft; 3, Aircraft; 51, Stresses and loads). Copies obtainable from Supt. of Docs., GPO, Washington	I. Mugler, John P., Jr. II. NASA TR R-58 NASA

TECHNICAL REPORT R–58

CALCULATION OF AERODYNAMIC LOADING AND TWIST CHARACTERISTICS OF A FLEXIBLE WING AT MACH NUMBERS APPROACHING 1.0 AND COMPARISON WITH EXPERIMENT

By JOHN P. MUGLER, JR.

SUMMARY

An iteration method is presented by which the detailed aerodynamic loading and twist characteristics of a flexible wing with known elastic properties may be calculated. The method is applicable at Mach numbers approaching 1.0 as well as at subsonic Mach numbers. Calculations are made for a wing-body combination; the wing was swept back 45° and had an aspect ratio of 4. Comparisons are made with experimental results at Mach numbers from 0.80 to 0.98. The calculated and experimental loadings and twist distributions are in good agreement at a Mach number of 0.80 at low angles of attack. With increases in angle of attack or Mach number, separation and mixed-flow phenomena cause the agreement between the calculated and experimental results to become poor.

INTRODUCTION

The aerodynamic loading on a flexible lifting surface is greatly affected by the structural deformations caused by the loading. Therefore, the calculation of the aerodynamic loading on a flexible surface is complicated by the fact that the elastic characteristics of the surface must be taken into consideration in order to obtain a good estimate of the resultant aerodynamic loading. References 1 to 3 present methods developed for the calculation of the aerodynamic loading on flexible wings. These methods are based on lifting-line concepts and a detailed theoretical description of the flow cannot be obtained. Since the boundary conditions for the lifting-line theory are satisfied at only one point on the chord, aeroelastic deformations in the chordwise direction cannot be taken into account in the calculations.

Presented herein is an iterative method, based on lifting-surface concepts, for the calculation of the aerodynamic loading on flexible wings. For lifting-surface theory, the boundary conditions are satisfied at several points on the chord, and the effects of chordwise deformations are accounted for in the calculations. The results yield both a detailed theoretical description of the flow on the flexible surface and the shape of the aeroelastically distorted surface.

Calculations were made by the method described herein for a wing-body combination; the wing was tapered and had a low aspect ratio. Theoretical and experimental results are compared at Mach numbers from 0.80 to 0.98.

SYMBOLS

a_{nm}	coefficients in expression for lift
c	section chord
$\bar{c}$	wing mean aerodynamic chord
c_{av}	average chord
c_l	section lift coefficient, $\frac{l}{qc}$
c_m	section pitching-moment coefficient, $\frac{m}{qc^2}$
D	diameter
E	total downwash factor
f	downwash factors for trailing vortex
G_{nr}	chordwise replacement load
g	downwash factors for bound vortex
K	kernel function

l section lift, $\int_0^c \Delta l\, dx$

Δl lift at any point

M free-stream Mach number

m section pitching moment about $c/4$, $\int_0^c \Delta l\left(\frac{c}{4}-x\right)dx$

Δp difference between lower-surface pressure and upper-surface pressure

q free-stream dynamic pressure

r body radius

$\bar{r}$ dimensionless body radius with respect to s_v

S wing area

s wing semispan

s' unsupported semispan (lateral distance from outer face of wing mounting block to tip)

s_v semispan of vortex

t tangent of angle of sweep of load lines

V free-stream velocity

w downwash velocity

X distance from midchord line to lift point

x, y longitudinal and lateral coordinates, respectively

$\bar{x}, \bar{y}$ dimensionless coordinates, x/s_v and y/s_v, respectively

$\frac{x_{cp}}{c}$ wing-section center of pressure measured from leading edge

y' lateral distance from outer face of wing mounting block

α angle of attack

$\Delta\alpha$ difference between angle of attack of wing station and angle of attack of wing-body center line

$\beta=\sqrt{1-M^2}$

η dimensionless coordinate, y/s

η' dimensionless coordinate, y'/s'

$\theta=\cos^{-1}\frac{X}{c/2}$

C_{ij} wing-twist influence coefficients due to normal loads at $c/4$

D_{ij} wing-twist influence coefficients due to moments about $c/4$

Subscripts:

a index of control points

b index of lift point or vortex

Matrix notation:

$\{\ \}$ column matrix

$[\ ]$ square matrix

$[\ ]^{-1}$ reciprocal matrix

METHOD

The method presented herein may be outlined as follows:

(1) Calculate the aerodynamic loading on the rigid wing using lifting-surface theory. The known built-in angle-of-attack distribution over the surface is used to define the boundary conditions.

(2) Use the elastic properties of the surface in conjunction with the aerodynamic loading from step (1) to calculate a new angle-of-attack distribution over the surface (corrected for aeroelastic deflections).

(3) Repeat steps (1) (using the corrected angle-of-attack distribution) and (2) until the aerodynamic and structural forces are in equilibrium. The results yield both the detailed aerodynamic loading on the aeroelastically distorted surface and the surface shape under load.

AERODYNAMIC LOADING ON RIGID WING

The lifting-surface theory outlined in reference 4 was used to calculate the aerodynamic loading on the rigid wing. The integral equation that relates a known downwash distribution to an unknown lift distribution may be written as

$$w(x_a,y_a)=\frac{1}{4\pi}\iint_S \Delta l(x_b,y_b)\boldsymbol{K}(x_a-x_b,y_b-y_a)dx_b/y_b \tag{1}$$

In equation (1), $w(x_a,y_a)$ is the downwash velocity at the point (x_a,y_a); $\boldsymbol{K}$ is the kernel function and represents the contribution to the downwash at the point (x_a,y_a); and $\Delta l(x_b,y_b)$ is the unknown lift distribution or local doublet strength associated with a pressure doublet of unit strength located at any point (x_b,y_b). In reference 4 the wing surface is replaced by a network of horseshoe vortices. The unknown loading is assumed to be expressible as a series of loading terms each weighted by an unknown coefficient to be determined. The series expression for the loading is used to obtain a set of chordwise replacement loads to represent the strength of each vortex. The downwash per unit

load produced by each vortex is expressed analytically as a downwash factor. Through this procedure the integral equation can be approximated by the summation (see eq. (14) of ref. 4)

$$w(x_a, y_a)=\frac{4s_r V}{\pi c}\sum_{\mu=1}^{s/s_r}\sum_{\nu=1}^{Q}\sum_{n=0}^{R} G_{n\nu}s\sqrt{1-\eta^2}\,(a_{n0}+a_{n1}\eta+\ldots a_{nm}\eta^m)E(\bar{x}_a, M, \theta_\nu, \bar{y}_\mu-\bar{y}_a) \tag{2}$$

where a_{nm} represents the unknown coefficients, $G_{n\nu}$, the replacement loads, and E, the downwash factors. In order to determine the values of the unknown coefficients a_{nm}, a set of control points is selected equal to the number of unknown coefficients. Then, if equation (2) is written for each control point and if the downwash angle w/V is equated to the slope of the mean camber line at each control point, a set of linear simultaneous equations results from which the unknown coefficients a_{nm} can be determined. This set of simultaneous equations can be written in matrix form as

$$\{B\}=[E]\{A\} \tag{3}$$

In equation (3) the elements of the column matrix $\{B\}$ are the slopes of the mean camber line at each control point and are defined as

$$\{B\}=\begin{vmatrix}\tan\alpha_1\\ \tan\alpha_2\\ \cdot\\ \cdot\\ \cdot\\ \tan\alpha_p\end{vmatrix} \tag{4}$$

The elements of the square matrix $[E]$ are the products of the downwash factors and the replacement loads and are defined as

$$\left[E\right]=\frac{4s_r}{\pi c}\begin{vmatrix}\sum_{\mu=1}^{s/s_r}\sum_{\nu=1}^{Q} G_{0\nu}s\sqrt{1-\eta^2}E(\bar{x}_1,M,\theta_\nu,\bar{y}_\mu-\bar{y}_1) & \sum_{\mu=1}^{s/s_r}\sum_{\nu=1}^{Q} G_{0\nu}s\sqrt{1-\eta^2}E(\bar{x}_1,M,\theta_\nu,\bar{y}_\mu-\bar{y}_1)\eta\ldots\\ \sum_{\mu=1}^{s/s_r}\sum_{\nu=1}^{Q} G_{0\nu}s\sqrt{1-\eta^2}E(\bar{x}_2,M,\theta_\nu,\bar{y}_\mu-\bar{y}_2) & \sum_{\mu=1}^{s/s_r}\sum_{\nu=1}^{Q} G_{0\nu}s\sqrt{1-\eta^2}E(\bar{x}_2,M,\theta_\nu,\bar{y}_\mu-\bar{y}_2)\eta\ldots\\ \cdots & \cdots\\ \sum_{\mu=1}^{s/s_r}\sum_{\nu=1}^{Q} G_{0\nu}s\sqrt{1-\eta^2}E(\bar{x}_p,M,\theta_\nu,\bar{y}_\mu-\bar{y}_p) & \sum_{\mu=1}^{s/s_r}\sum_{\nu=1}^{Q} G_{0\nu}s\sqrt{1-\eta^2}E(\bar{x}_p,M,\theta_\nu,\bar{y}_\mu-\bar{y}_p)\eta\ldots\end{vmatrix}$$

$$\begin{vmatrix}\ldots\sum_{\mu=1}^{s/s_r}\sum_{\nu=1}^{Q} G_{0\nu}s\sqrt{1-\eta^2}E(\bar{x}_1,M,\theta_\nu,\bar{y}_\mu-\bar{y}_1)\eta^m\ldots & \sum_{\mu=1}^{s/s_r}\sum_{\nu=1}^{Q} G_{n\nu}s\sqrt{1-\eta^2}E(\bar{x}_1,M,\theta_\nu,\bar{y}_\mu-\bar{y}_1)\eta^m\\ \ldots\sum_{\mu=1}^{s/s_r}\sum_{\nu=1}^{Q} G_{0\nu}s\sqrt{1-\eta^2}E(\bar{x}_2,M,\theta_\nu,\bar{y}_\mu-\bar{y}_2)\eta^m\ldots & \sum_{\mu=1}^{s/s_r}\sum_{\nu=1}^{Q} G_{n\nu}s\sqrt{1-\eta^2}E(\bar{x}_2,M,\theta_\nu,\bar{y}_\mu-\bar{y}_2)\eta^m\\ \cdots & \cdots\\ \ldots\sum_{\mu=1}^{s/s_r}\sum_{\nu=1}^{Q} G_{0\nu}s\sqrt{1-\eta^2}E(\bar{x}_p,M,\theta_\nu,\bar{y}_\mu-\bar{y}_p)\eta^m\ldots & \sum_{\mu=1}^{s/s_r}\sum_{\nu=1}^{Q} G_{n\nu}s\sqrt{1-\eta^2}E(\bar{x}_p,M,\theta_\nu,\bar{y}_\mu-\bar{y}_p)\eta^m\end{vmatrix} \tag{5}$$

The column matrix $\{A\}$ contains the unknown coefficients and the elements are defined as

$$\{A\}=\begin{vmatrix} a_{00} \\ a_{01} \\ \cdot \\ \cdot \\ \cdot \\ a_{0m} \\ \cdot \\ \cdot \\ \cdot \\ a_{nm} \end{vmatrix} \tag{6}$$

From equation (3) the unknown coefficients a_{nm} can be obtained by solving the following equation:

$$\{A\}=[E]^{-1}\{B\} \tag{7}$$

Since the elements of $[E]^{-1}$ can be calculated and since the elements of $\{B\}$ are known from the built-in angle-of-attack distribution, the unknown coefficients in $\{A\}$ can be evaluated from equation (7). The effects of the presence of a central body are accounted for by multiplying the slopes in $\{B\}$ and the downwash due to the bound leg of the vortex in the calculation for $[E]^{-1}$ in equation (7) by the factor $[1+(\bar{r}^2/y_a^2)]$. (See ref. 4.)

The coefficients determined from equation (7) can now be used to calculate the aerodynamic parameters c_l and c_m (appendix C, ref. 4) as follows:

$$c_l=\frac{4\tan\alpha s\pi}{c}\sqrt{1-\eta^2}\,[2(a_{00}+\eta^2 a_{02}+\ldots\eta^m a_{0m}) +(a_{10}+\eta^2 a_{12}+\ldots\eta^m a_{1m})] \tag{8}$$

and

$$c_m=-\frac{s\pi\tan\alpha}{c^2}\sqrt{1-\eta^2}\,[(a_{10}+\eta^2 a_{12}+\ldots\eta^m a_{1m}) -(a_{20}+\eta^2 a_{22}+\ldots\eta^m a_{2m})] \tag{9}$$

where the moments are taken about $c/4$ instead of about $c/2$ as in reference 4. The parameters of equations (8) and (9) define the rigid-wing aerodynamic loading and will be used to determine a corrected angle-of-attack distribution.

CORRECTED ANGLE-OF-ATTACK DISTRIBUTION

The change in angle at each control point, due to the aerodynamic loading of equations (8) and (9), can now be calculated using the relation

$$\{\Delta\alpha\}=[C]\{P\}+[D]\{T\} \tag{10}$$

The elements of the column matrix $\{\Delta\alpha\}$ are the changes in the angle at each control point and are defined as

$$\{\Delta\alpha\}=\begin{vmatrix} \Delta\alpha_1 \\ \Delta\alpha_2 \\ \cdot \\ \cdot \\ \cdot \\ \Delta\alpha_p \end{vmatrix} \tag{11}$$

The structural-deflection influence coefficients are the elements of the square matrices $[C]$ and $[D]$. The elements C_{ij} and D_{ij} are the twist at the ith station due to a unit normal load at the jth station and the twist at the ith station due to a unit moment at the jth station, respectively. The elements of the column matrices $\{P\}$ and $\{T\}$ are the integrated loads and moments, respectively, over the jth spanwise segment; that is,

$$P_j=qs'\int_{\frac{j-1}{N}}^{\frac{j}{N}} c_l c\,d\eta' \tag{12}$$

and

$$T_j=qs'\int_{\frac{j-1}{N}}^{\frac{j}{N}} c_m c^2\,d\eta' \tag{13}$$

where N is the number of segments. The values of c_l and c_m to be used in equations (12) and (13) are obtained from equations (8) and (9), respectively.

The results of equation (10) (i.e., the changes in slopes at the various control points due to the aerodynamic loading) are used to correct the slopes of the mean camber line previously used as elements of the column matrix $\{B\}$ in equation (7) (before the body factor is applied). These corrected slopes define the new angle-of-attack distribution corrected for aeroelastic distortions.

ITERATION

The new angle-of-attack distribution is now substituted in equation (7) to determine a new set of coefficients a_{nm}. These new coefficients are in

turn used in equations (8) and (9) to determine a new aerodynamic loading. This loading is then used in equation (10) to determine further changes in the slopes at each of the control points. The process is repeated until there are no further changes in the loadings of equations (8) and (9). The loading obtained from this iteration process is the loading on the deformed wing. Also, the angle-of-attack distribution used to obtain this loading defines the shape of the deformed surface.

CALCULATIONS

Calculations have been made for the wing-body combination shown in figure 1. The wing has a sweepback of 45° of the 0.25c line, an aspect ratio of 4.0, and a taper ratio of 0.15. The wing has an NACA 65A206, $a=0$ airfoil section at the root and varies linearly in thickness to an NACA 65A203, $a=0.8$ (modified) airfoil section at the 0.50 semispan station; the thickness ratio remains constant to the tip.

This particular wing was chosen because the results of references 5 and 6 show that it underwent rather large aeroelastic distortions at the test conditions. For example, at a Mach number of 0.98 and an angle of attack of 4°, the tip twist was −3.54° during tests at 1 atmosphere stagnation pressure (table VII, ref. 5). In other words, the wing tip was operating at only 0.46° when the wing-body center line was at 4°. Large aeroelastic distortions have a large effect on the spanwise load distributions, as noted in reference 6.

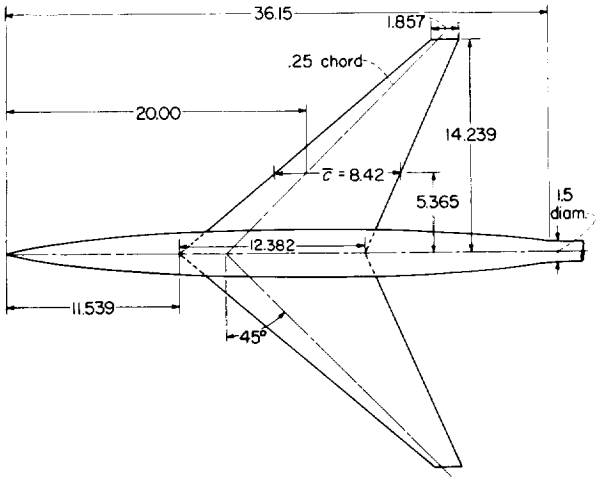

Wing details

Area, sq ft	1.408
Aspect ratio	4
Taper ratio	0.15
Dihedral, deg	0

FIGURE 1.—Details of wing-body combination. All dimensions are in inches unless otherwise noted.

The central body shown in figure 1 was represented in the calculations as an infinite cylinder with a diameter equal to the maximum diameter of the fuselage (3.212 inches). In making the calculations, the vortex pattern with 12 control points and four load lines located as shown in figure 2 was used. This vortex pattern divides the wing into intervals of 0.1 semispan except in the region of the tip where the corrector vortex was placed and near the central body where fractional vortices were employed. In the calculations for the downwash factor E, the relations of the appendix were used. These relations differ from those given in reference 4 in that the bound leg of the horseshoe vortices is considered to be swept-back to coincide with the sweepback of the load lines. As previously mentioned, the slopes used in the column matrix $\{B\}$ of equation (7) are the slopes of the mean camber line at each control point. Influence coefficients were obtained for this wing from a static calibration and are presented in table I. The influence coefficients were obtained along the $c/4$, $c/2$, and $3c/4$ lines so that the changes in slope at all the control points, which were also located along these constant-chord lines, could be calculated.

The calculations were programed for the IBM 704 electronic data processing machine at the Langley Research Center. Generally, five iterations were necessary at each test condition for the aerodynamic and structural forces to be in equilibrium. The machine time required was about ¾ minute for each test condition. The calculations were made at four Mach numbers, $M=0.80$, 0.90, 0.94, and 0.98, for a stagnation pressure of 1 atmosphere. The results are linear with angle of attack so that only enough calculations to define the rate of change of the significant parameters with angle of attack were necessary. The results are presented at constant angles of attack for convenience in comparing the calculated data with the experimental data.

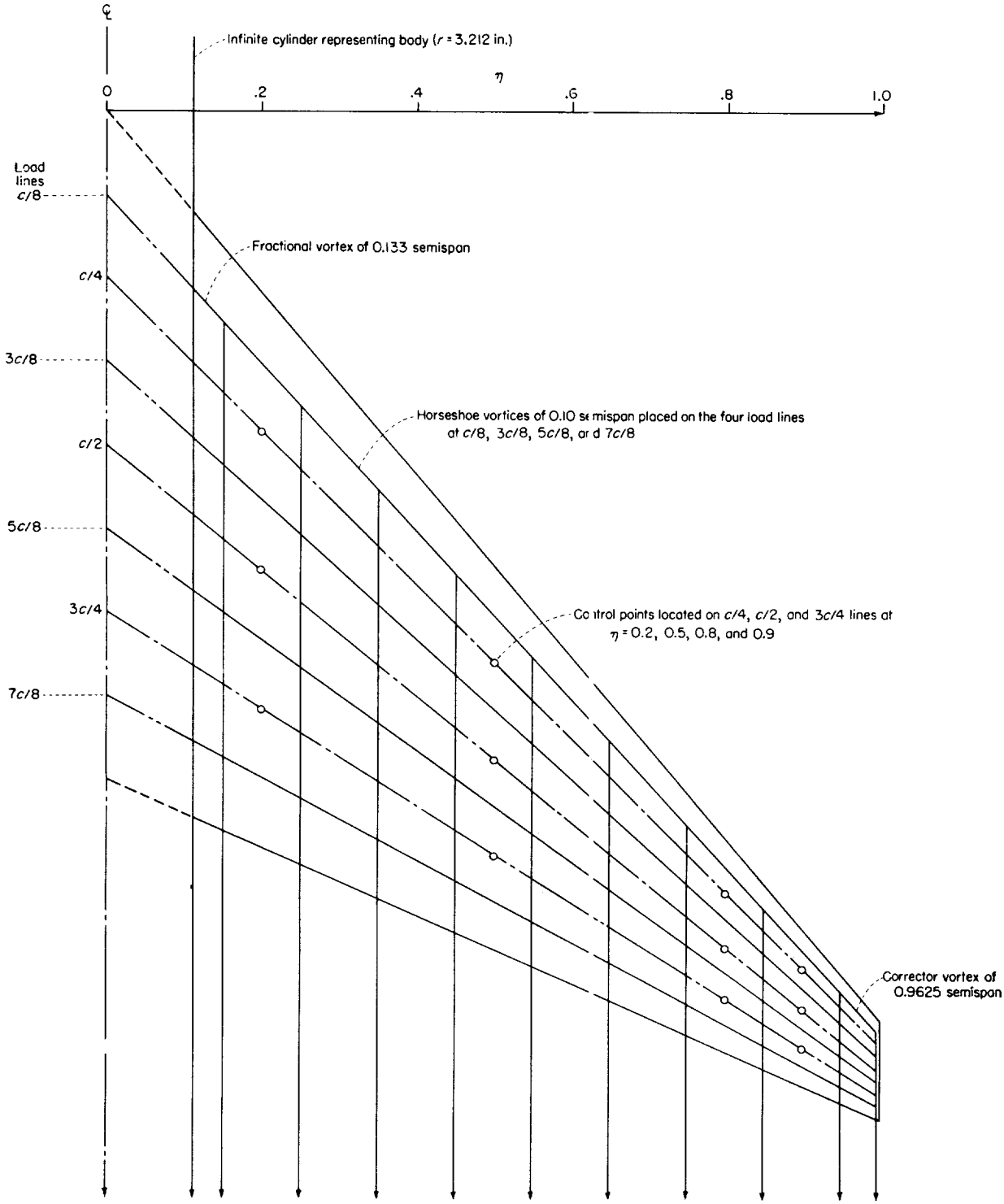

FIGURE 2.—Vortex pattern for wing showing control-point locations.

COMPARISON OF EXPERIMENTAL AND THEORETICAL RESULTS

Experimental data obtained on the configuration shown in figure 1 were presented in references 5 and 6 and are used herein for comparisons with theoretical results. All the experimental data used herein were obtained at a stagnation pressure of 1 atmosphere.

SPAN LOAD CHARACTERISTICS

A comparison of the experimental and theoretical span load distributions is presented in figure 3. At a Mach number of 0.80 (fig. 3(a)) and at angles of attack of 0°, 2°, and 4° the theoretical and experimental results are in good agreement. At angles of attack of 8°, −2°, and −4°, the agreement is poor. Examination of the experimental chordwise pressure distributions of reference 5 indicates that at these latter angles of attack, a leading-edge separation vortex is formed on the wing which has significantly altered the character of the flow. Viscous effects were not taken into account in the theoretical calculations, so prediction of this type of distribution should not be expected. With increases in Mach number to 0.98 (fig. 3(d)), the agreement at 0° angle of attack remains fairly good. However, the agreement becomes poor with increases in angle of attack to 2° and 4°. At the Mach numbers of 0.90, 0.94, and 0.98, the experimental data of reference 5 show that the flow over a major portion of the upper surface of the wing is supersonic, the extent being dependent on both angle of attack and Mach number. This flow characteristic is one factor in accounting for the poor predictions at these Mach numbers and angles. It was pointed out in reference 7 that the method for performing the

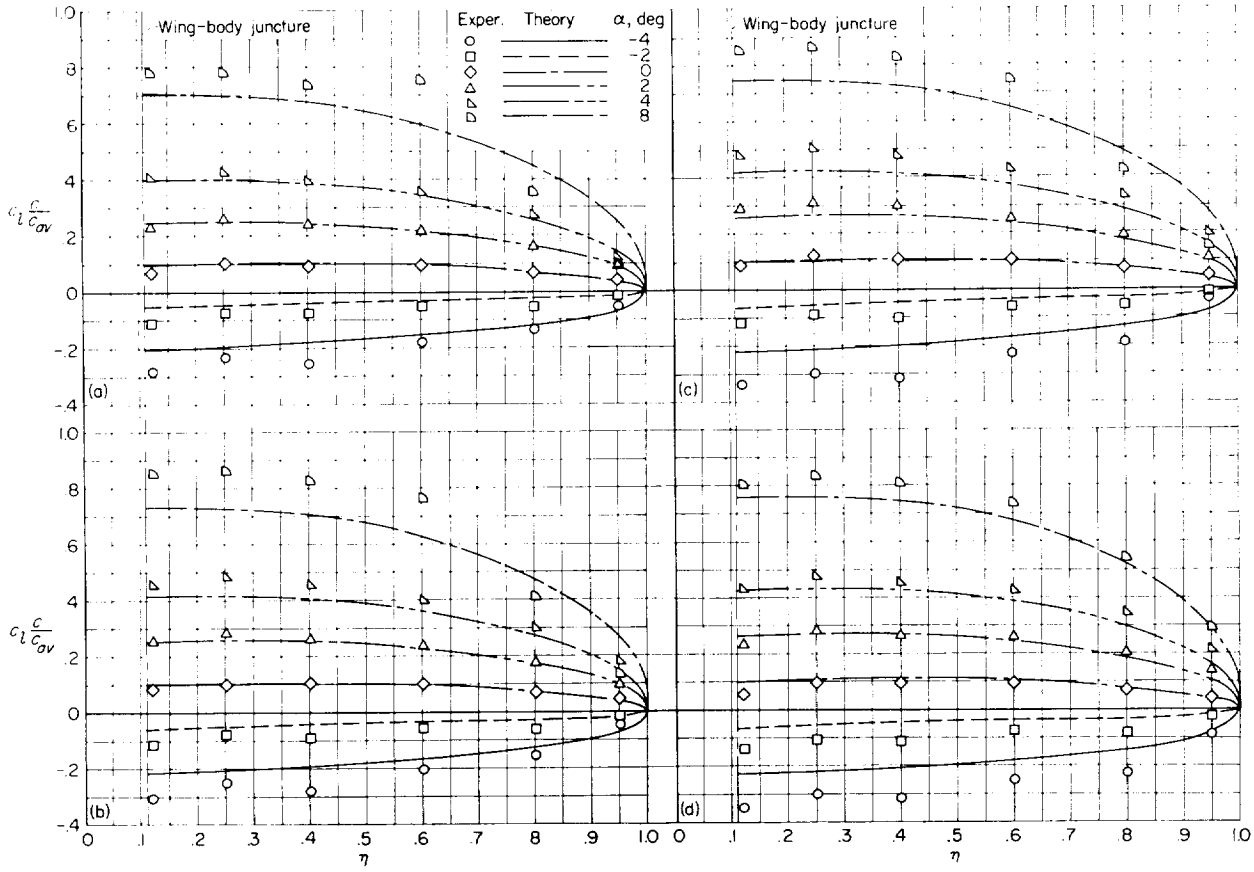

(a) $M=0.80$.
(b) $M=0.90$.
(c) $M=0.94$.
(d) $M=0.98$.

FIGURE 3.—Comparison of experimental and theoretical span load distributions for flexible wing.

chordwise integrations by the use of replacement loads (given in ref. 4) breaks down for this wing plan form as the Mach number approaches 1.0. This factor may also account for the poor predictions at Mach numbers close to 1.0.

TWIST CHARACTERISTICS

A comparison of the experimental and theoretical twist distributions along the $c/4$, $c/2$, and $3c/4$ lines is presented in figure 4 for a Mach number of 0.80. In general, the agreement is good at angles of attack from $-2°$ to $4°$ in each case. Figure 4 also shows that there is little difference in the twist characteristics at the three chordwise stations for this wing. Figure 5 presents the comparison of experimental and theoretical twist distributions along the $c/4$ line at the three higher Mach numbers. The agreement is still good at angles of attack from $-2°$ to $4°$ at Mach numbers of 0.90 and 0.94; however, at $M=0.98$, the agreement is poor at all angles other than $0°$.

CHORDWISE CENTER-OF-PRESSURE CHARACTERISTCS

A comparison of the experimental and theoretical chordwise center-of-pressure location at an angle of attack of $4°$ is shown in figure 6. In general, the agreement is good over the inboard 0.8 of the span up to a Mach number of about 0.90.

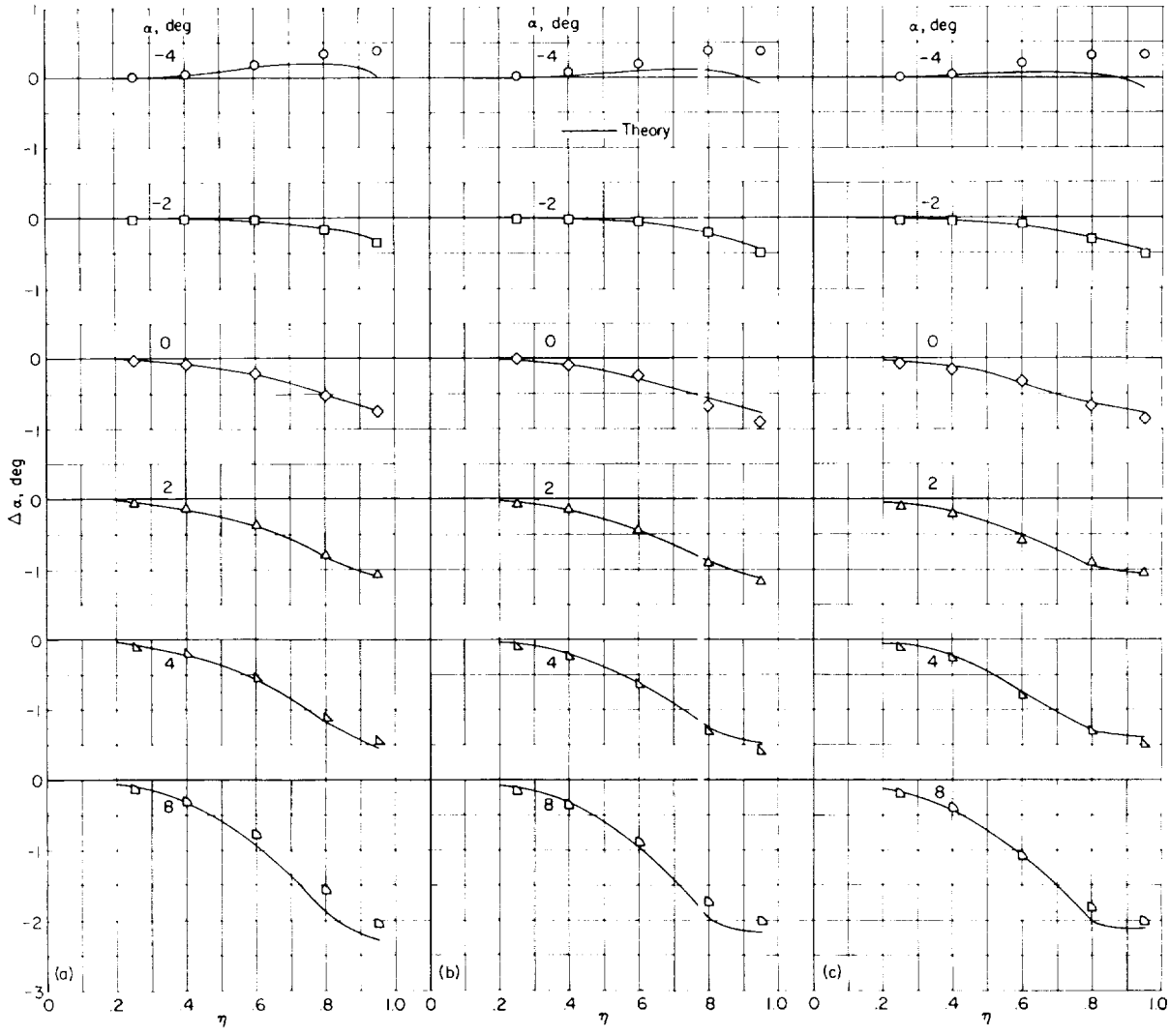

(a) Twist along $c/4$ line. (b) Twist along $c/2$ line. (c) Twist along $3c/4$ line.

FIGURE 4.—Comparison of experimental and theoretical twist distributions. $M=0.80$.

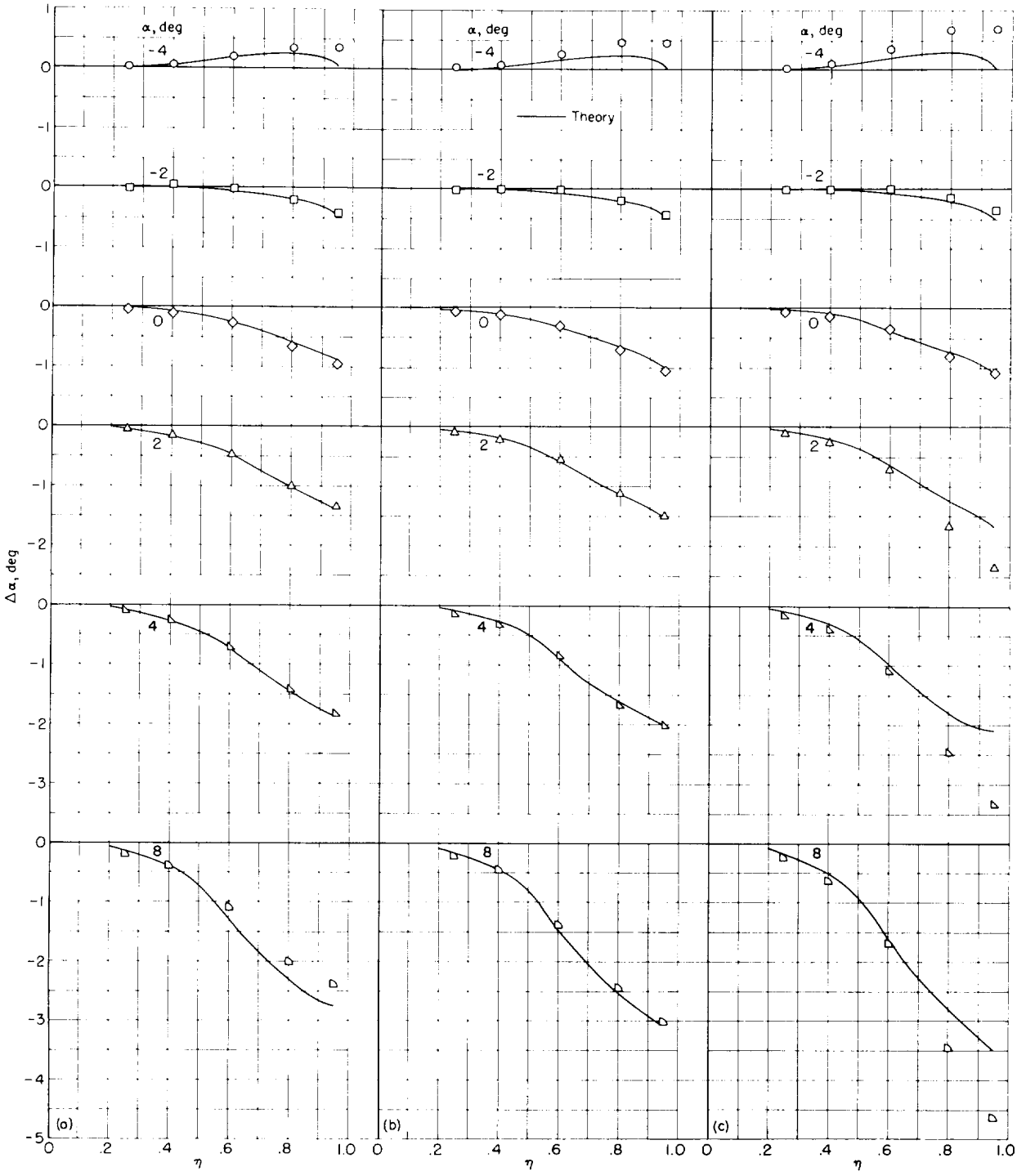

(a) $M=0.90$. (b) $M=0.94$. (c) $M=0.98$.

FIGURE 5.—Comparison of experimental and theoretical twist distributions along c/4 line.

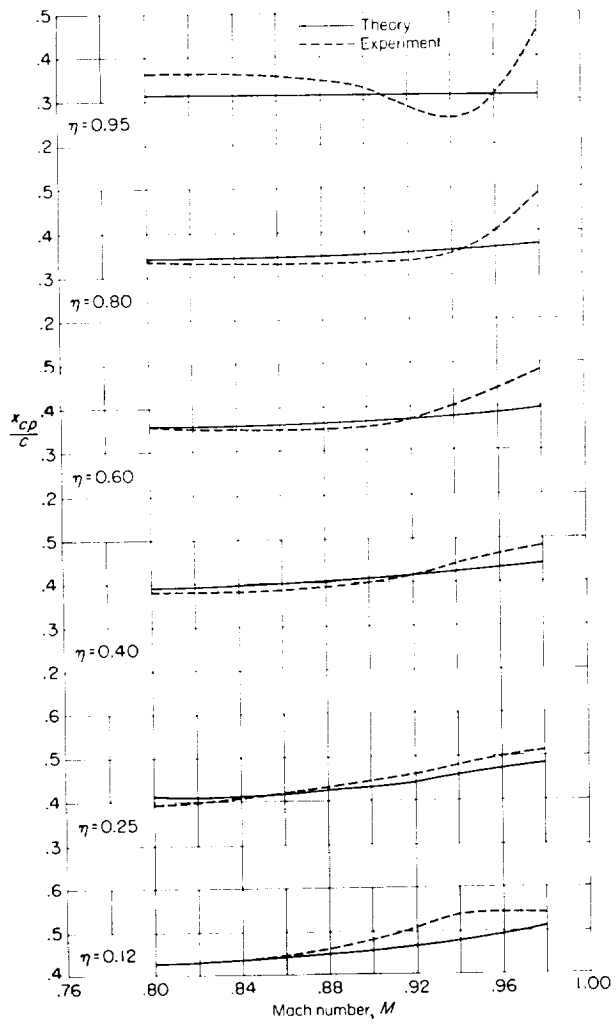

FIGURE 6.—Comparison of experimental and theoretical chordwise center-of-pressure location. $\alpha=4°$.

At a Mach number of 0.80, the chordwise pressure distributions in reference 5 indicate that separation was occurring at the 0.95 semispan station at $\alpha=4°$. This separation accounts for the discrepancy between the experimental and theoretical results at this condition. At a Mach number of 0.98, the experimental location was rearward of the theoretical location over the entire span. The distributions of reference 5 show that at this test condition, a supersonic distribution developed over the trailing-edge region and was responsible for the rearward center-of-pressure movement. This rearward location is also responsible for the large disagreement between the experimental and theoretical twist distributions at $M=0.98$ in figure 5.

PRESSURE DISTRIBUTIONS

Several chordwise pressure distributions have been calculated to determine if the good agreement obtained for the other parameters at $M=0.80$ was indicative of good agreement in the pressure distributions. Figure 7 presents a comparison of experimental and theoretical chordwise lifting pressure distribution at four spanwise stations and at three angles of attack. The agreement is generally good.

CONCLUSIONS

An iteration method is presented by which the detailed aerodynamic loading and twist characteristics of a flexible wing with known elastic properties may be calculated. The method is applicable at Mach numbers approaching 1.0 as well as at subsonic Mach numbers. Calculations were made for a combination of a body and a cambered wing with 45° sweepback, an aspect ratio of 4, a taper ratio of 0.15, and a thickened root section. Comparisons of experimental and calculated results at Mach numbers from 0.80 to 0.98 indicate the following conclusions:

1. At a Mach number of 0.80, the calculated and experimental loadings and the wing twist distributions were in good agreement from 0° to 4° angle of attack. At higher positive angles and at negative angles, the experimental data indicated that separation was prominent on the wing and the agreement between calculated and experimental results was poor.

2. With increases in Mach number, the agreement between calculated and experimental results at 2° and 4° angle of attack became succeedingly poorer. At 0° angle of attack the agreement was still good at a Mach number of 0.98. The experimental data indicated that the poorer agreement at angles of attack of 2° and 4° for the higher Mach number was the result of large regions of mixed flow which developed on the wing.

LANGLEY RESEARCH CENTER,
NATIONAL AERONAUTICS AND SPACE ADMINISTRATION,
LANGLEY FIELD, VA., *August 14, 1959.*

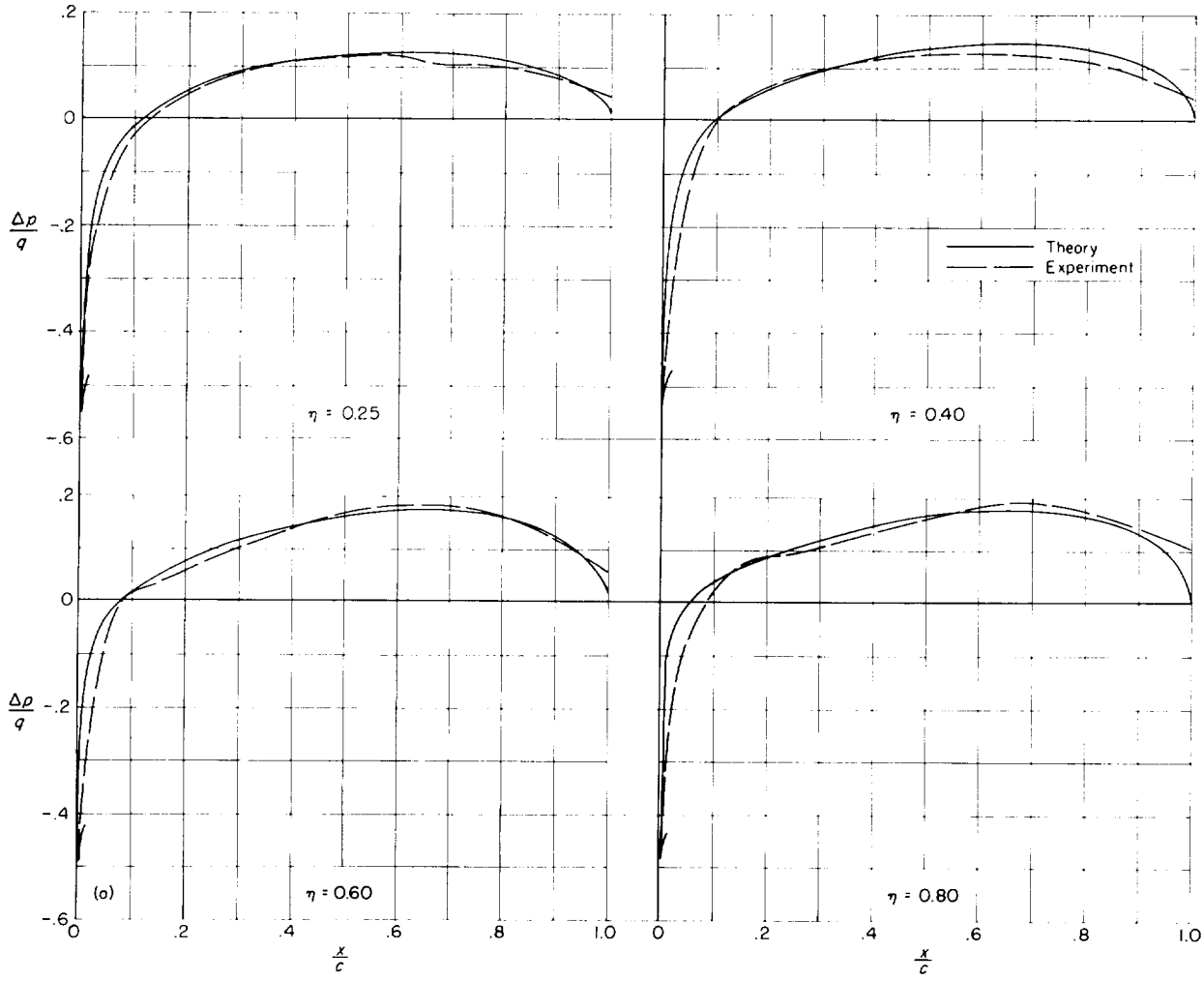

(a) $\alpha=0°$.

FIGURE 7.—Comparison of experimental and theoretical chordwise lifting pressure distribution. $M=0.80$.

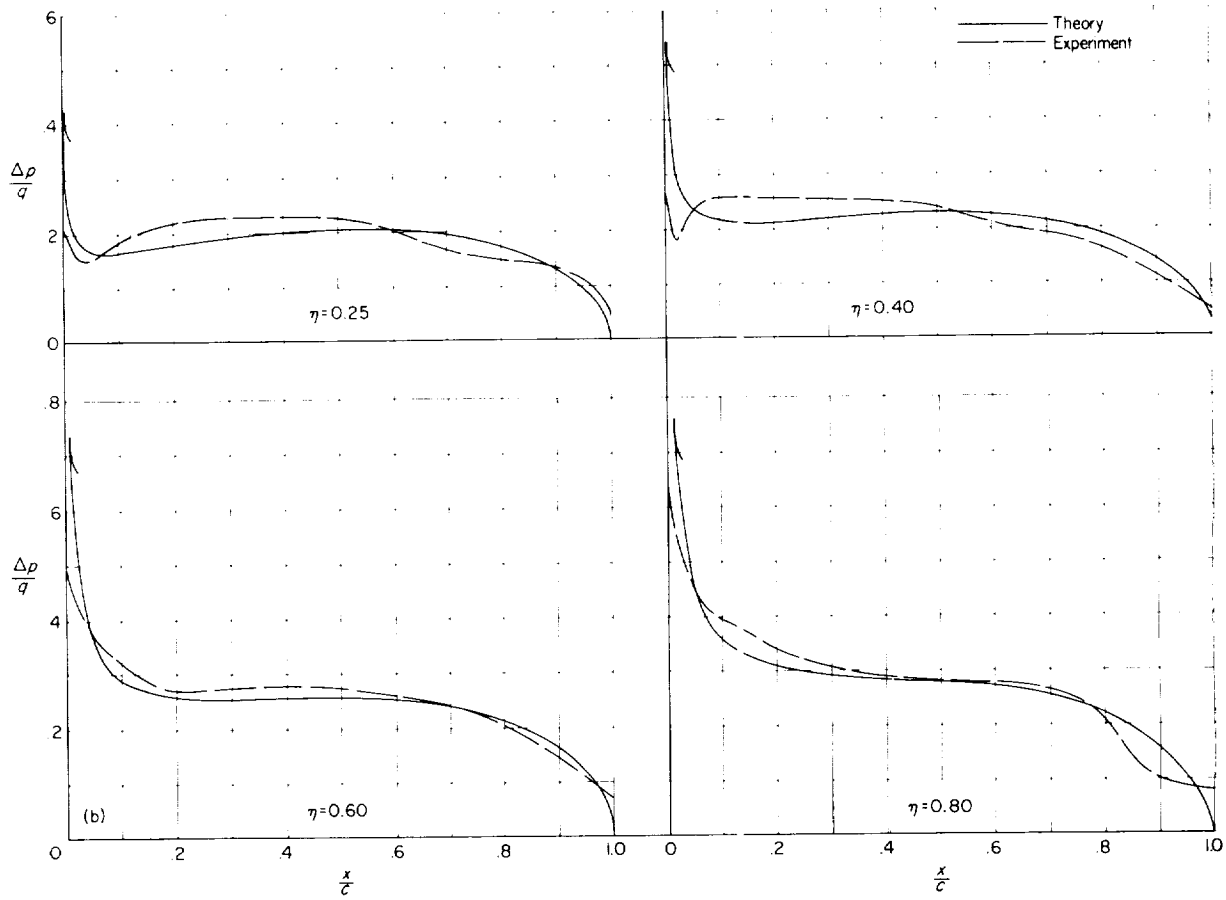

(b) $\alpha = 2°$.

FIGURE 7.—Continued.

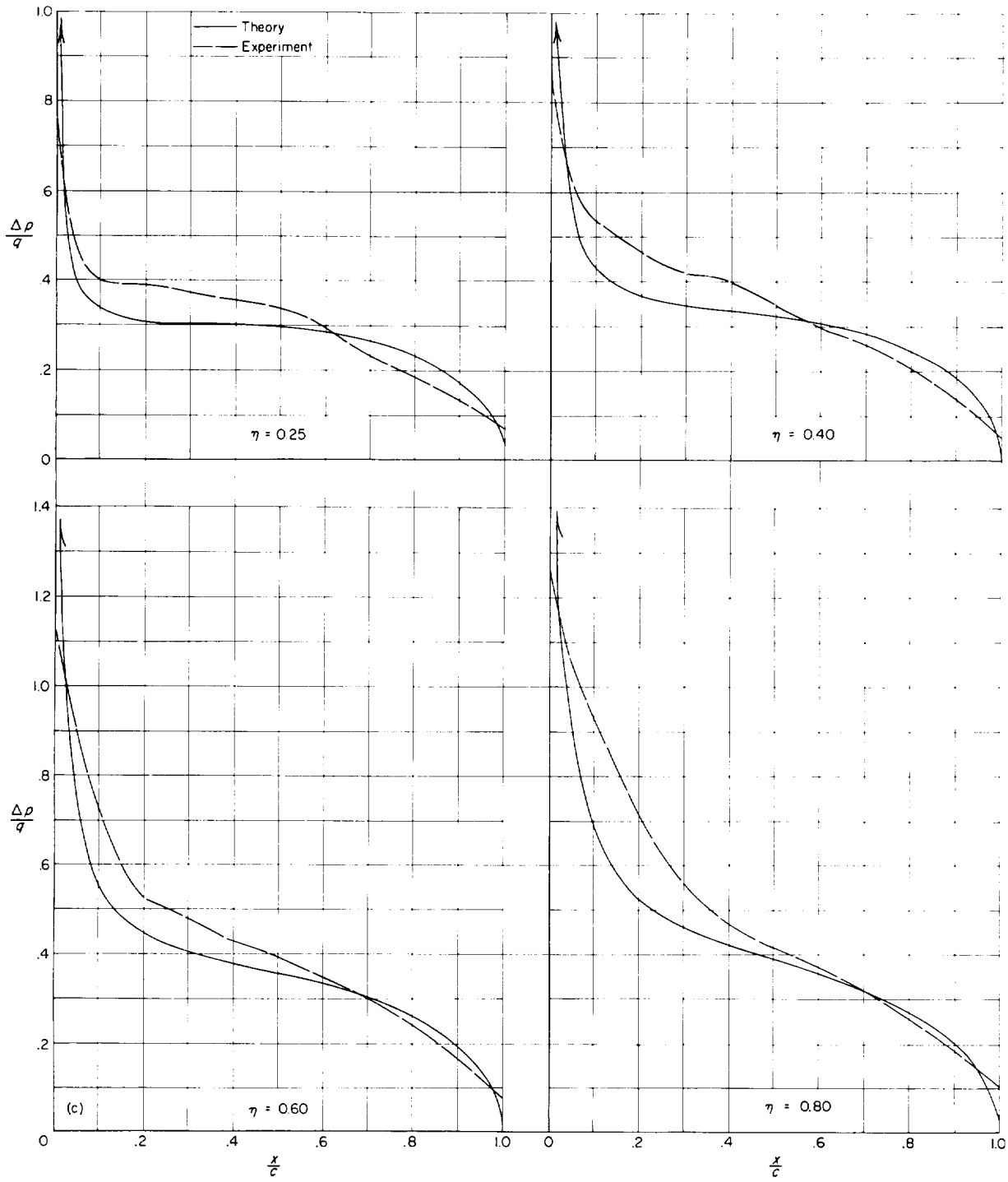

(c) $\alpha = 4°$.

FIGURE 7.—Concluded.

APPENDIX

RELATIONS USED TO CALCULATE DOWNWASH

In the relations given in appendix A of reference 4 the bound leg of the horseshoe vortices representing the wing-body combination is considered to be normal to the free stream. In order to make the expression for the downwash exact, the sweepback of the wing must be included in deriving the expressions. Recent unpublished work by John L. Crigler of the Langley Research Center has shown that better agreement with experimental results is obtained when the downwash is calculated with the bound leg of the horseshoe vortices swept back to coincide with the load lines. Therefore, these exact downwash expressions were used in the calculations made herein and are presented below. Since a correction is applied to the downwash associated with the bound leg of the vortex, it is desirable to calculate the contribution due to the trailing and bound legs separately. These relations are nondimensional with all distances referred to s_v. The sum of the contributions of the bound and trailing legs of the vortex (width $2s_v$) at point (x_b,y_b) to the downwash factor at point (x_a,y_a) is given by

$$f_{ba}+g_{ba}=\frac{1}{(\bar{y}_b-\bar{y}_a+1)}\frac{1}{s_v}\left[\frac{(\bar{x}_a-\bar{x}_b)+t(\bar{y}_b-\bar{y}_a)+\sqrt{(\bar{x}_a-\bar{x}_b-t)^2+\beta^2(\bar{y}_b-\bar{y}_a+1)^2}}{(\bar{x}_a-\bar{x}_b)+t(\bar{y}_b-\bar{y}_a)}\right]$$
$$-\frac{1}{(\bar{y}_b-\bar{y}_a-1)}\frac{1}{s_v}\left[\frac{(\bar{x}_a-\bar{x}_b)+t(\bar{y}_b-\bar{y}_a)+\sqrt{(\bar{x}_a-\bar{x}_b+t)^2+\beta^2(\bar{y}_b-\bar{y}_a-1)^2}}{(\bar{x}_a-\bar{x}_b)+t(\bar{y}_b-\bar{y}_a)}\right] \quad \text{(A1)}$$

The contribution of only the trailing legs of the vortex at point (x_b,y_b) and of width $2s_v$ to the downwash factor at point (x_a,y_a) is given by

$$f_{ba}=\frac{1}{(\bar{y}_b-\bar{y}_a+1)}\frac{1}{s_v}\left[\frac{(\bar{x}_a-\bar{x}_b-t)+\sqrt{(\bar{x}_a-\bar{x}_b-t)^2+\beta^2(\bar{y}_b-\bar{y}_a+1)^2}}{\sqrt{(\bar{x}_a-\bar{x}_b-t)^2+\beta^2(\bar{y}_b-\bar{y}_a+1)^2}}\right]$$
$$-\frac{1}{(\bar{y}_b-\bar{y}_a-1)}\frac{1}{s_v}\left[\frac{(\bar{x}_a-\bar{x}_b+t)+\sqrt{(\bar{x}_a-\bar{x}_b+t)^2+\beta^2(\bar{y}_b-\bar{y}_a-1)^2}}{\sqrt{(\bar{x}_a-\bar{x}_b+t)^2+\beta^2(\bar{y}_b-\bar{y}_a-1)^2}}\right] \quad \text{(A2)}$$

and

$$g_{ba}=(f_{ba}+g_{ba})-f_b \quad \text{(A3)}$$

The contribution to the downwash factor at the point (x_a,y_a) due to the vortex at point $(x_b,-y_b)$ for a wing with symmetrical loading $\Delta l(x_b,y_b)=\Delta l(x_b,-y_b)$ is given by

$$f'_{ba}+g'_{ba}=\frac{1}{(\bar{y}_b+\bar{y}_a+1)}\frac{1}{s_v}\left[\frac{(\bar{x}_a-\bar{x}_b)+t(\bar{y}_b-\bar{y}_a)+\sqrt{(\bar{x}_a-\bar{x}_b-t)^2+\beta^2(\bar{y}_b+\bar{y}_a+1)^2}}{(\bar{x}_a-\bar{x}_b)+t(\bar{y}_b+\bar{y}_a)}\right]$$
$$-\frac{1}{(\bar{y}_b+\bar{y}_a-1)}\frac{1}{s_v}\left[\frac{(\bar{x}_a-\bar{x}_b)+t(\bar{y}_b-\bar{y}_a)+\sqrt{(\bar{x}_a-\bar{x}_b+t)^2+\beta^2(\bar{y}_b+\bar{y}_a-1)^2}}{(\bar{x}_a-\bar{x}_b)+t(\bar{y}_b+\bar{y}_a)}\right] \quad \text{(A4)}$$

and

$$f'_{ba}=\frac{1}{(\bar{y}_b+\bar{y}_a+1)}\frac{1}{s_r}\left[\frac{(\bar{x}_a-\bar{x}_b-t)+\sqrt{(\bar{x}_a-\bar{x}_b-t)^2+\beta^2(\bar{y}_b+\bar{y}_a+1)^2}}{\sqrt{(\bar{x}_a-\bar{x}_b-t)+\beta^2(\bar{y}_b+\bar{y}_a+1)^2}}\right]$$

$$-\frac{1}{(\bar{y}_b+\bar{y}_a-1)}\frac{1}{s_r}\left[\frac{(\bar{x}_a-\bar{x}_b+t)+\sqrt{(\bar{x}_a-\bar{x}_b+t)^2+\beta^2(\bar{y}_b+\bar{y}_a-1)^2}}{\sqrt{(\bar{x}_a-\bar{x}_b+t)^2+\beta^2(\bar{y}_b+\bar{y}_a-1)^2}}\right] \quad (A5)$$

Therefore,

$$g'_{ba}=(f'_{ba}+g'_{ba})-f'_{ba} \quad (A6)$$

In calculating the downwash velocities from the image vortices, it was found that consideration of the sweepback of the bound leg of the vortex had a negligible effect on the results because the width of the image vortices is small compared with the width of the wing vortices. Therefore, the slope of the bound leg was not included in the image calculations and the remainder of the downwash factor was calculated by the method of reference 4.

REFERENCES

1. Diederich, Franklin W.: Calculation of the Aerodynamic Loading of Swept and Unswept Flexible Wings of Arbitrary Stiffness. NACA Rep. 1000, 1950.
2. Gaugh, William J., and Slap, Joseph K.: Determination of Elastic Wing Aerodynamic Characteristics. Jour. Aero. Sci., vol. 19, no. 3, Mar. 1952, pp. 173–182.
3. Gray, W. L., and Schenk, K. M.: A Method for Calculating the Subsonic Steady-State Loading on an Airplane With a Wing of Arbitrary Plan Form and Stiffness. NACA TN 3030, 1953.
4. Crigler, John L.: Comparison of Calculated and Experimental Load Distributions on Thin Wings at High Subsonic and Sonic Speeds. NACA TN 3941, 1957.
5. Mugler, John P., Jr.: Basic Pressure Measurements at Transonic Speeds on a Thin 45° Sweptback Highly Tapered Wing With Systematic Spanwise Twist Variations Untwisted Wing. NASA MEMO 10-20-58L, 1958.
6. Fischetti, Thomas L.: Investigation at Mach Numbers From 0.80 to 1.43 of Pressure and Load Distributions Over a Thin 45° Sweptback Highly Tapered Wing in Combination With Basic and Indented Bodies. NACA RM L57D29a, 1957.
7. Crigler, John L.: A Method for Calculating Aerodynamic Loadings on Thin Wings at a Mach Number of 1. NASA TN D-96, 1959.

TABLE I.—INFLUENCE COEFFICIENTS

(a) Along $c/4$ line

Twist measurement station, η	Wing-twist influence coefficients due to normal loads at $c/4$, C_{ij}, deg/lb, at—				
	$\eta'=0.185$	$\eta'=0.348$	$\eta'=0.565$	$\eta'=0.795$	$\eta'=0.948$
0.25	−0.0001	−0.0002	−0.0005	−0.0014	−0.0040
.40	0	−.0002	−.0011	−.0032	−.0088
.60	.0003	−.0002	−.0014	−.0129	−.0215
.80	.0003	−.0001	−.0015	−.0182	−.0638
.95	.0005	0	−.0014	−.0173	−.0950

Twist measurement station, η	Wing-twist influence coefficients due to moments about $c/4$, D_{ij}, deg/in-lb, at—				
	$\eta'=0.185$	$\eta'=0.348$	$\eta'=0.565$	$\eta'=0.795$	$\eta'=0.948$
0.25	0.0001	0.0001	0.0002	0.0004	−0.0009
.40	.0001	.0004	.0009	.0015	−.0029
.60	.0002	.0006	.0020	.0048	.0098
.80	.0003	.0007	.0039	.0186	.0334
.95	.0003	.0007	.0043	.0237	.1136

(b) Along $c/2$ line

Twist measurement station, η	Wing-twist influence coefficients due to normal loads at $c/4$, C_{ij}, deg/lb, at—				
	$\eta'=0.185$	$\eta'=0.348$	$\eta'=0.565$	$\eta'=0.795$	$\eta'=0.948$
0.25	0	−0.0002	−0.0007	−0.0012	0.0013
.40	0	−.0001	−.0016	.0040	.0066
.60	0	.0001	−.0011	.0125	−.0239
.80	0	−.0001	.0009	−.0167	.0716
.95	0	−.0001	−.0009	−.0156	.0835

Twist measurement station, η	Wing-twist influence coefficients due to moments about $c/4$, D_{ij}, deg/in-lb, at—				
	$\eta'=0.185$	$\eta'=0.348$	$\eta'=0.565$	$\eta'=0.795$	$\eta'=0.948$
0.25	0.0002	0.0002	0.0002	0.0002	0
.40	.0002	.0005	.0008	.0008	0
.60	.0002	.0007	.0040	.0050	.0047
.80	.0002	.0007	.0042	.0233	.0383
.95	.0002	.0007	.0041	.0258	.1453

TABLE I.—INFLUENCE COEFFICIENTS—Concluded

(c) Along $3c/4$ line

Twist measurement station, η	Wing-twist influence coefficients due to normal loads at $c/4$, C_{ij}, deg/lb, at—				
	$\eta' = 0.185$	$\eta' = 0.348$	$\eta' = 0.565$	$\eta' = 0.795$	$\eta' = 0.948$
0.25	0	−0.0001	−0.0008	−0.0019	−0.0027
.40	0	−.0001	−.0012	−.0048	−.0066
.60	0	−.0001	−.0011	−.0154	−.0305
.80	0	−.0001	−.0009	−.0165	−.0716
.95	0	−.0001	−.0009	−.0153	−.0725

Twist measurement station, η	Wing-twist influence coefficients due to moments about $c/4$, D_{ij}, deg/in-lb, at—				
	$\eta' = 0.185$	$\eta' = 0.348$	$\eta' = 0.565$	$\eta' = 0.795$	$\eta' = 0.948$
0.25	0.0002	0.0004	0.0005	0.0004	0
.40	.0002	.0007	.0015	.0016	.0023
.60	.0002	.0007	.0038	.0088	.0081
.80	.0002	.0007	.0043	.0252	.0637
.95	.0001	.0006	.0050	.0252	.1434

U.S. GOVERNMENT PRINTING OFFICE: 1960